

# The effects of spatially distributed damping on the contact force in railway pantograph-catenary interactions

Yang Song, *Member, IEEE*, Tengjiao Jiang, Anders Rønnquist, Petter Nåvik, Gunnstein Frøseth

**Abstract**— According to field measurements, the damping ratio of a railway catenary varies along the span length and shows an inherent uncertainty. In numerical simulations, it is common to assume a constant damping ratio. Herein, a methodology is proposed to include the variable damping ratio of a catenary in numerical simulations of pantograph-catenary interactions. The damping ratios of the catenary are extracted from the measurement uplifts of critical points along the span, including the droppers, the steady arm and the stitch wires. The absolute nodal coordinate formulation is utilised to model the catenary. The geometric nonlinearity of the contact and messenger wires, the dropper slackness and the initial configuration are appropriately described. The damping ratio coefficients of each element within one span are obtained by interpolation using smoothing splines. A variable time step is adopted in the numerical simulations to accurately capture the contact loss duration. The numerical analysis indicates that the damping ratio variation mainly affects the local behaviours of contact forces with high cut-off frequencies. Particularly, the trailing pantograph contact loss duration evaluated with a constant damping ratio is significantly different from the result with a variable damping ratio. **The damping coefficients are assumed to follow the Gaussian distribution, of which the mean and standard deviation are obtained from multiple measurements.** The stochastic analysis results show that the damping ratio uncertainty should be considered when evaluating the high-frequency maximum contact force and the contact loss of the trailing pantograph at high speed. Otherwise, a large error may be expected when using a constant damping ratio.

**Index Terms**—Electrified Railway, Pantograph-catenary interaction, Contact force, Damping ratio variation, Contact loss

## I. INTRODUCTION

In recent years, the impressive expansion of the electrified railway network around the world is a direct reflection of the global tendency towards the incremental demand for fast transport from all aspects of the economy and society. Fundamental research on vehicle dynamics and their interaction with infrastructure has attracted ever-increasing attention from the industrial and academic communities, as they are the main factors that ensure the reliable operation of railways and determine the maximum speed of high-speed trains. The

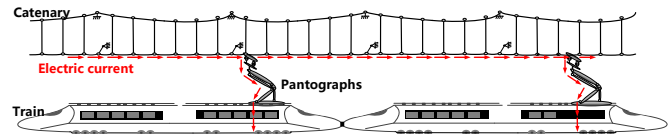


Figure 1. Description of a pantograph-catenary system

catenary constructed along a railroad is responsible for transmitting electric current to the locomotive by sliding contact with pantographs. As shown in Figure 1, a catenary is a stationary mechanical system used for transmitting electric current to moving pantographs. The contact quality between the registration strip of the pantograph and the contact wire of the catenary directly determines the current collection quality of an electric train. Therefore, a good pantograph-catenary interaction performance is preferred to ensure stable contact and safe operation of an electric railway.

Mathematical modelling has been widely used to reproduce realistic behaviours of pantograph-catenary interaction [1], as it is an efficient way to validate design strategies and an essential approach to facilitate fundamental research on pantograph-catenary dynamics. As speeds increase, the important implication of catenary damping on pantograph-catenary interactions has attracted increasing attention [2]. Particularly, when the electric motor unit (EMU) is equipped with double pantographs, catenary damping has a nonnegligible effect on the behaviour of the trailing pantograph [3]. The structural damping identified from measurement data can be used in numerical models to evaluate pantograph-catenary responses. The latest validation standard [4] specifies that catenary damping should be considered in numerical simulations and provides a nondimensional damping rate (the ratio of damping vs. critical damping) for a reference model of a catenary. Referring to the standard form of Rayleigh damping, the damping matrix can be expressed as

$$\mathbf{C}_c^G = \alpha \mathbf{M}_c^G + \beta \mathbf{K}_c^G \quad (1)$$

where  $\mathbf{M}_c^G$ ,  $\mathbf{K}_c^G$  and  $\mathbf{C}_c^G$  are the global mass, stiffness and damping matrices of the catenary, respectively; and  $\alpha$  and  $\beta$  are the damping coefficients, which are defined as  $1.25 \times 10^{-2} \text{ s}^{-1}$  and  $1.0 \times 10^{-4} \text{ s}$  in the standard, respectively. However, due to

Manuscript received xxxx; revised xxxx; accepted xxxx. Date of publication xxxx; date of current version xxxx. This work was supported in part by the National Natural Science Foundation of China (U1734202).

Yang Song, Tengjiao Jiang, Anders Rønnquist, Petter Nåvik, Gunnstein Frøseth are with the Department of Structural Engineering, Norwegian

University of Science and Technology, Trondheim, 7491, Norway. (e-mail: y.song\_ac@hotmail.com, tengjiao.jiang@ntnu.no, anders.ronnquist@ntnu.no, petter.r.navik@ntnu.no, gunnstein.t.froseth@ntnu.no).

structural complexity and nonlinearity, the damping ratio along the catenary may not always be constant. Even though the damping variation along the span length may not have a substantial effect on the overall dynamics of the catenary, it may influence the local behaviour, especially the local fluctuations in contact forces and contact losses, which are essential factors to assess current collection quality. Furthermore, the real-life damping ratio variation may affect the reliability of the catenary. Deterministic assessment indices [5] are incapable of evaluating current collection quality with random parameters. Therefore, the variation and uncertainty of the structural damping should be involved in numerical simulations to evaluate the pantograph-catenary interaction performance.

The last decade has witnessed the rapid development of catenary modelling techniques [6]. The ever-increasing speed on railways has necessitated an accurate description of wave propagation in catenary models [7]. Therefore, the mode superposition method has been widely used to model catenaries [8] due to its economic computational cost. Currently, the finite element method (FEM) is the most preferred method to model catenaries, as it can properly describe the initial configuration [9], the contact wire pre-sag [10] and the nonlinearity [11]. Appropriate modelling of external disturbances on the catenary has recently attracted the interest of the scientific community. The vehicle vibration [12], [13], the wind load [14] and the ice coating [15] have been properly included in numerical models to evaluate their effects on the current collection quality. Different from the traditional structures subjected to wind load [16], [17], the wind may cause the aerodynamic instability of catenaries [18], which interrupts the operation of the railway and causes potential destructive damage to the catenary. Maintenance has been an important part of the research field in recent years. Modelling of degradation is helpful to evaluate the service performance of a pantograph-catenary system in different service periods. Wear [19], height variations [20], [21] and component defects [22], [23] have been introduced in numerical simulations to investigate their impacts on the initial configuration and the current collection quality. To address the stochastics in these disturbances, Monte Carlo (MC) simulations have been used to conduct a stochastic analysis of dynamic performance [24]. Based on numerical results, the optimisation strategies of catenaries [25], [26] and control schemes of pantographs [27], [28] have been proposed to ensure a stable and safe operation of pantograph-catenary systems.

To improve the accuracy of numerical simulations, measurement data have been widely used to modify numerical models. N avik et al [29] first utilised a recorded acceleration time series to identify the structural damping of a catenary based on the covariance-driven stochastic subspace identification (Cov-SSI) method. Similar works were performed by Zou et al [2] and Duan et al [30] to identify the Rayleigh coefficients of catenaries in China's high-speed railway network. The summarised damping can be directly used in numerical simulations, and the results indicate that catenary damping has a non-negligible effect on pantograph-catenary

interactions at high speed [31]. Xu et al [3] demonstrated that catenary damping had a direct impact on the dynamic behaviour of the trailing pantograph, which was normally disturbed by the travelling wave excited by the leading pantograph. To the best of the authors' knowledge, previous research has adopted a constant damping ratio in numerical simulations. This assumption should be improved as the damping ratio along a catenary has been proven to vary along the span length in field measurements. This work also indicated that there is a significant variation in the damping ratio, which should be included in numerical simulations of pantograph-catenary interactions.

From the above literature review, it is seen that not only the variation in catenary damping along the span length but also the dispersion of the damping ratio at one point have not previously been considered in numerical simulations. This paper addresses these issues by presenting a methodology that includes a realistic damping ratio variation obtained from field measurements in the numerical model of a catenary. The catenary is modelled by a nonlinear finite element approach [32], which can simulate the pantograph-catenary behaviour at frequencies of up to 200 Hz. The effect of damping ratio variation on the interaction performance is investigated. Considering the damping ratio uncertainty, MC simulations are conducted to evaluate the interaction performance of a pantograph-catenary system with random parameters.

## II. DESCRIPTION OF DAMPING RATIO VARIATION

To obtain the realistic damping ratio of a catenary, the vertical uplifts of some critical points along the whole span, including the droppers, the steady arm and the stitch wires, are measured from the Gardemobanen line. This section gives a brief introduction of the data acquisition and damping identification approaches.

The catenary uplifts are measured by the noncontact vision-based line-tracking system called VIBLITE, which was developed in [33]. In contrast to traditional contact-based sensors [34], VIBLITE can be placed beside a railroad at a safe distance from the track without disturbing normal operations. The purpose of the system is to measure line-like elements in a large variety of backgrounds. The joints of six droppers and the steady arm point are selected as sampling points, as shown in Figure 2. To fully describe the damping ratio dispersion, at least five train passages are measured at each point. The Cov-SSI method [35] is adopted to identify the modal frequencies and damping ratios from the measurement data. The Rayleigh damping coefficients  $\alpha$  and  $\beta$  are obtained by curve fitting of the damping ratio vs frequency with a 95% confidence interval. Figure 3 presents boxplots for the distribution of  $\alpha$  and  $\beta$  along a one-span catenary obtained from five measurements. In contrast to the previous assumption of a constant damping ratio coefficient, the mean  $\alpha$  and  $\beta$  show a significant variation along the span. The maximum  $\alpha$  appears at the first and last dropper positions, whereas the maximum  $\beta$  appears at the mid-span dropper positions. In Section IV, the mean  $\alpha$  and  $\beta$  are included in the numerical simulations to compare the resulting pantograph-catenary contact force (PCCF) with that obtained



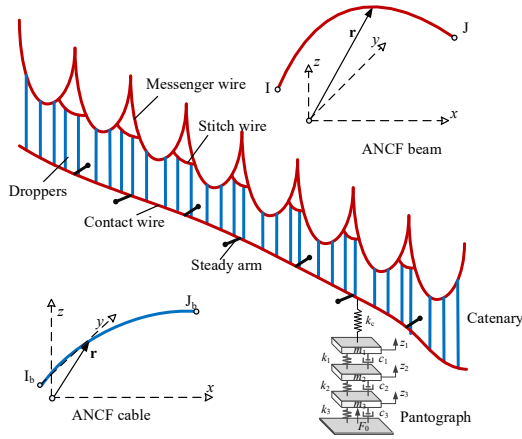


Figure 4. Catenary model based on ANCF beam and cable elements. Red lines denote the ANCF beam element, and blue lines denote the ANCF cable element

$$\Delta \mathbf{F}^G = \mathbf{K}_T^G \Delta \mathbf{U}_C + \mathbf{K}_L^G \Delta \mathbf{L}_0 \quad (8)$$

where  $\Delta \mathbf{F}^G$  is the global unbalanced force vector and  $\mathbf{K}_T^G$  and  $\mathbf{K}_L^G$  are the global stiffness matrices related to the incremental nodal displacement vector  $\Delta \mathbf{U}_C$  and the incremental unstrained length vector  $\Delta \mathbf{L}_0$ , respectively. It is seen that  $[\mathbf{K}_T^G \quad \mathbf{K}_L^G]$  is not a square matrix. The total number of unknowns in Eq. (8) exceeds the total number of equations, which leads to undetermined solutions. Hence, additional constraint conditions should be introduced to suppress undesired movements, according to the design specifications. These additional constraints can also reduce  $[\mathbf{K}_T^G \quad \mathbf{K}_L^G]$  to a square matrix and ensure that Eq. (8) has unique solutions. The details of the additional constraints can be found in [37]. In this way, the strained and unstrained lengths of all the elements are calculated, and the initial configuration of the catenary can be determined. Introducing a consistent mass matrix and damping matrix, the equation of motion for the catenary system is written as

$$\mathbf{M}_C^G \ddot{\mathbf{U}}_C(t) + \mathbf{C}_C^G \dot{\mathbf{U}}_C(t) + \mathbf{K}_C^G(t) \mathbf{U}_C(t) = \mathbf{F}_C^G(t) \quad (9)$$

The pantograph is modelled by a lumped-mass model. A penalty function method is utilised to couple the two systems. Based on the assumption of the relative penetration generated between the two contact surfaces, the contact force  $f_c$  can be calculated by

$$f_c = \begin{cases} k_s \delta & \text{if } \delta > 0 \\ 0 & \text{if } \delta \leq 0 \end{cases} \quad (10)$$

in which the penetration  $\delta$  can be evaluated by

$$\delta = z_1 - z_c \quad (11)$$

where  $z_1$  and  $z_c$  are the vertical displacements of the pantograph head and the contact wire, respectively. The friction is not considered in the model as it has no significant contribution to the contact force [38]. In the dynamic simulation of pantograph-catenary interaction, the iteration is performed in each time step.  $z_1$  and  $z_c$  are calculated by

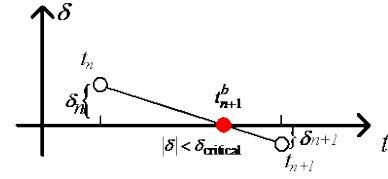


Figure 5. Description of variable time step scheme

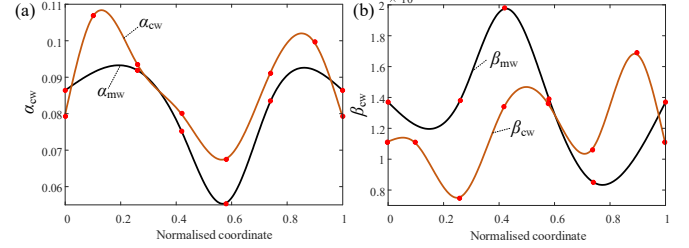


Figure 6. Curve fitting of damping coefficients against normalised coordinates: (a)  $\alpha$  and (b)  $\beta$ . Red points denote measurement damping coefficients. Solid lines represent fitted curves using smoothing spline

exerting the contact force  $f_c$  on the catenary model and pantograph model, respectively. Through the penetration assumption,  $f_c$  is updated according to  $z_1$  and  $z_c$ . In the first time step, the pantograph is lifted to contact with the contact wire, and calculate the static contact force and the initial displacement.

To accurately describe the separation and reattachment of the pantograph head and the contact wire, a variable time step is adopted in the numerical simulations. As shown in Figure 5, contact loss is assumed to occur within the time step  $t_n \rightarrow t_{n+1}$ . To capture the separation time instant, a tangent line  $l$  is drawn to calculate the intersection point  $t_{n+1}^b$  with the time axis. Accordingly, the time step is updated to  $\Delta t^b = t_{n+1} - t_{n+1}^b$  to calculate the penetration  $\delta$  at  $t_{n+1}^b$ . This procedure can be repeated until a proper penetration  $|\delta| < \delta_{critical}$  is obtained. In this work, the threshold  $\delta_{critical}$  is defined as  $10^{-6}$  m. A similar procedure is also used to capture the reattachment time instant.

To validate the numerical model, a numerical example is implemented by comparison with the measurement data from the "Gardermobanen" rail line in Norway, going from Oslo to Eidsvoll. The inspection vehicle regularly runs at 160 km/h. This speed is adopted in this validation and the subsequent analyses. The pantograph on the roof of an inspection train is WBL 85. The comparison with the measurement data is presented in Table 1. It is seen that the maximum error of the simulation result against the measurement data reaches

Table 1. Dynamic validation of the present model against measurement data

	Measurement	Present model	Error
Mean [N]	92.14	92.34	0.22%
Std. (0-20 Hz) [N]	11.53	10.59	8.15%
Std. (0-5 Hz) [N]	9.01	8.86	1.66%
Std. (5-20 Hz) [N]	6.33	5.72	9.64%
Max. [N]	126.64	125.44	0.95%
Min. [N]	52.85	57.14	8.12%
Range of vertical position of the point of contact [mm]	78	68.5	12.18%

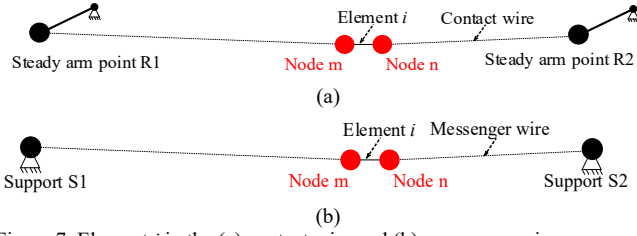
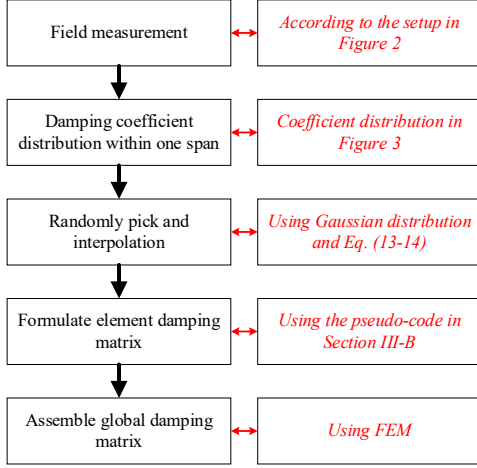

 Figure 7. Element  $i$  in the (a) contact wire and (b) messenger wire


Figure 8. Procedure to formulate catenary damping matrix

15.65%, which is still lower than the acceptance threshold of 20% specified in the standard [39].

### B. Inclusion of damping variation

In numerical simulations, the damping matrix  $\mathbf{C}_c^G$  obtained by Eq. (1) with constant  $\alpha$  and  $\beta$  cannot consider the damping ratio variation along the span. Taking the mean  $\alpha$  and  $\beta$  in Figure 3 as an example, this section illustrates the procedure to include the damping coefficient variation in the catenary model.

Due to the complexity of actual conditions, the catenary span length is not always the same. For the measured tensile section, the span length varies from 42.6 m to 63.3 m. The length for the measured span is 49.8 m, and it is impossible to measure all the spans due to the considerable working load. In this paper, the damping ratio variation is assumed to be identical for all spans. The longitudinal coordinate is normalised to 0-1, and the damping coefficients within two measurement points are obtained by the fitted curve using smoothing splines, as shown in Figure 6. Generally, the smoothing spline  $s$  for each damping coefficient is constructed for the specified smoothing parameter  $p$  and the specified weights  $w_i$  by

$$\min \left| p \sum w_i (\phi_i - s(\eta_i))^2 + (1-p) \int \left( \frac{d^2 s}{d\eta^2} \right)^2 d\eta \right| \quad (13)$$

where  $\eta_i$  is the normalised coordinate at the  $i^{\text{th}}$  measurement point and  $\phi_i$  is the damping coefficient  $\alpha$  or  $\beta$  at the  $i^{\text{th}}$  measurement point. The fitted curve  $\hat{f}(\eta)$  is a piecewise polynomial function, which can be used to calculate the damping coefficients within any two adjacent measurement points. Multiplying the normalised coordinate by the real span

length  $L_{sp}$  yields the fitting curves of the damping coefficient for all spans, which can be expressed as

$$f(x) = \hat{f}(x/L_{sp}) \quad (14)$$

where  $x$  is the local coordinate for one span and  $0 \leq x \leq L_{sp}$ .

Then, the following procedure is proposed to generate the damping matrix for each element. Consider that index  $i$  changes from 1 to the total element number  $N_{\text{element}}$ .

For  $i = 1 \rightarrow N_{\text{element}}$

If element  $i$  is in the contact wire:

- Obtain the longitudinal position of two nodes  $x_m$  and  $x_n$  of the element and two adjacent steady arm points  $x_{R1}$  and  $x_{R2}$ , as shown in Figure 7 (a).
- Calculate  $\alpha_{cw}^m$ ,  $\alpha_{cw}^n$ ,  $\beta_{cw}^m$ , and  $\beta_{cw}^n$  with Eq. (14).
- Formulate the element mass and stiffness matrices  $\mathbf{M}_{ei}$  and  $\mathbf{K}_{ei}$ , and calculate the element damping matrix  $\mathbf{C}_{ei}$  by

$$\mathbf{C}_{ei} = \begin{bmatrix} \alpha_{cw}^m \times 6 \times 12 & \times 6 \times 12 \\ \times 6 \times 12 & \times 6 \times 12 \\ \times 6 \times 12 & \times 6 \times 12 \\ \times 6 \times 12 & \times 6 \times 12 \end{bmatrix} + \begin{bmatrix} \times 6 \times 12 & \times 6 \times 12 \\ \times 6 \times 12 & \times 6 \times 12 \\ \times 6 \times 12 & \times 6 \times 12 \\ \times 6 \times 12 & \times 6 \times 12 \end{bmatrix}$$

Else if element  $i$  is in the messenger wire:

- Obtain the longitudinal position of two nodes  $x_m$  and  $x_n$  of the element and two adjacent supports  $x_{S1}$  and  $x_{S2}$ , as shown in Figure 7 (b).
- Calculate  $\alpha_{mw}^m$ ,  $\alpha_{mw}^n$ ,  $\beta_{mw}^m$ , and  $\beta_{mw}^n$  with Eq. (14).
- Formulate the element mass and stiffness matrices  $\mathbf{M}_{ei}$  and  $\mathbf{K}_{ei}$ , and calculate the element damping matrix  $\mathbf{C}_{ei}$  by

$$\mathbf{C}_{ei} = \begin{bmatrix} \alpha_{mw}^m \times 6 \times 12 & \times 6 \times 12 \\ \times 6 \times 12 & \times 6 \times 12 \\ \times 6 \times 12 & \times 6 \times 12 \\ \times 6 \times 12 & \times 6 \times 12 \end{bmatrix} + \begin{bmatrix} \times 6 \times 12 & \times 6 \times 12 \\ \times 6 \times 12 & \times 6 \times 12 \\ \times 6 \times 12 & \times 6 \times 12 \\ \times 6 \times 12 & \times 6 \times 12 \end{bmatrix}$$

Else if element  $i$  is in the stitch wire:

- Calculate  $\alpha_{sw}$  and  $\beta_{sw}$  from the mean values of the two measurement points in the stitch wire.
- Formulate the element mass and stiffness matrices  $\mathbf{M}_{ei}$  and  $\mathbf{K}_{ei}$ , and calculate the element damping matrix by

$$\mathbf{C}_{ei} = \alpha_{sw} \mathbf{M}_{ei} + \beta_{sw} \mathbf{K}_{ei}$$

End

End

The global damping matrix  $\mathbf{C}_c^G$  can be obtained by assembling all the element damping matrices  $\mathbf{C}_{ei}$  obtained in the above procedure. **The procedure to formulate the damping matrix is presented in Figure 8.** Note that the fitted curves of all damping coefficients in Figure 6 are obtained by the mean values of multiple measurements, which are taken as an example to illustrate the present procedure to include the damping ratio variation in the numerical model. The fitted curves in Figure 6 are adopted in Section IV to compare the contact forces obtained when using constant and variable damping ratios. **When the damping ratio uncertainty is considered in Section V, the fitted curves can be reconstructed**

Table 2. Catenary parameters

Total length	1.012 km
Contact wire tension	15 kN
Messenger wire tension	15 kN
Stitch wire tension	2.8 kN
Contact wire area	120 mm <sup>2</sup>
Messenger wire area	65.8 mm <sup>2</sup>
Stitch wire area	3.44 mm <sup>2</sup>
Contact wire linear density	1.07 kg/m
Messenger wire linear density	0.596 kg/m
Number of spans in contact with the pantograph	18

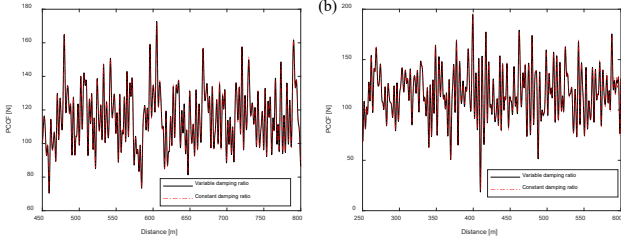


Figure 9. PCCFs filtered with a 20 Hz cut-off frequency with and without damping ratio variation: (a) leading pantograph and (b) trailing pantograph

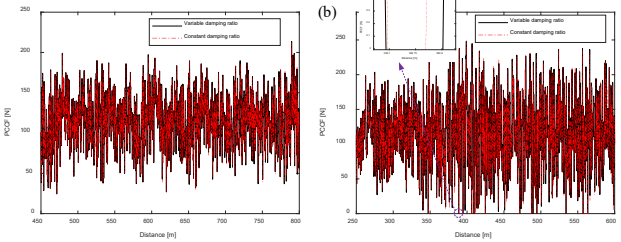


Figure 10. PCCFs filtered with a 200 Hz cut-off frequency with and without damping ratio variation: (a) leading pantograph and (b) trailing pantograph

via the random damping coefficients generated according to the normal distribution assumption.

#### IV. DYNAMIC PERFORMANCE WITH DAMPING RATIO VARIATION

The pantograph-catenary model is constructed according to the parameters of the measurement section from the Gardermoen line in Norway, which goes from Oslo to Eidsvoll. The parameters of the catenary for the analysis section are presented in Table 2. Pantograph WBL 85 is adopted in the simulations, and the lumped-mass parameters can be found in [40]. An operating speed of 220 km/h is adopted here to compare the PCCFs evaluated with and without damping ratio variation. In this work, a double pantograph operation with 200 m intervals is taken in the analysis. Double pantographs are widely used worldwide to ensure sufficient electric current is collected by the EMU. The trailing pantograph behaviour is more sensitive to structural damping, as it is directly affected by the catenary vibration excited by the leading pantograph.

According to the current standard [5], the PCCF filtered with a 20 Hz cut-off frequency can be used to assess the current collection quality. Based on this idea, the PCCFs for the leading and trailing pantographs with and without damping ratio variation are presented in Figure 9. For the leading and trailing pantographs, the PCCFs evaluated with and without damping

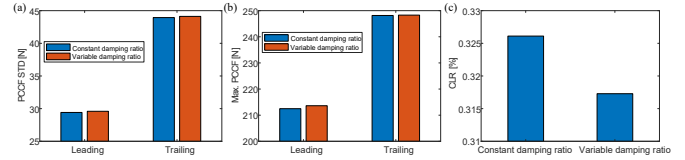


Figure 11. PCCF statistics with and without damping ratio variation: (a) PCCF standard deviation, (b) maximum PCCF, and (c) contact loss rate

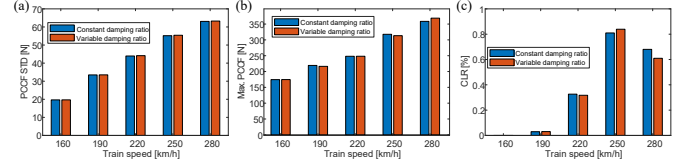


Figure 12. Trailing PCCF statistics at different speeds with and without damping ratio variation: (a) PCCF standard deviation, (b) maximum PCCF, and (c) contact loss rate

ratio variation do not show a distinct difference. Therefore, it can be concluded that the damping ratio variation does not affect the low-frequency behaviour of the pantograph-catenary interaction. It is not necessary to include the damping ratio variation in the evaluation of the PCCF filtered with a 20 Hz cut-off frequency according to the current standard.

The low cut-off frequency for the PCCF has been criticised by several scholars in recent years [32] as it loses essential information for describing the behaviour of pantograph-catenary interactions. Generally, the common view is to improve the frequency of interest up to 200 Hz, as it can fully describe the minimal contact loss duration (5 ms) specified in EN 50367 [5]. The suggestions in [32] are adopted in this analysis to simulate the PCCF at frequencies of up to 200 Hz. The PCCFs filtered with a 200 Hz cut-off frequency with and without damping ratio variation are presented in Figure 10. The waveforms of the PCCF evaluated by the two approaches are similar. However, for the trailing pantograph, some local behaviours of the PCCF are significantly changed when the variable damping ratio is included. In particular, the contact loss duration evaluated with a constant damping ratio is different from that with a variable damping ratio, as demonstrated in the locally enlarged view in Figure 10 (b).

To further compare the PCCF with and without damping ratio variation, the statistics of the PCCF filtered with a 200 Hz cut-off frequency are presented in Figure 11. The maximum value and the standard deviation do not experience a significant change when the damping ratio variation is included. However, a relatively larger difference can be seen in the contact loss rate. The contact loss rate decreases from 0.367% to 0.357% when the variable damping ratio is included. For the given case, the traditional method with a constant damping ratio leads to more conservative results.

According to EN 50119 [41], the maximum speed for the analysed catenary can be calculated by 0.7 times its wave propagation speed; hence, the maximum speed is approximately 280 km/h. In this section, the train speeds vary from 160 km/h to 280 km/h with a 30 km/h interval to perform numerical simulations to compare the PCCFs evaluated with and without damping ratio variation. The above analysis indicates that the structural damping ratio variation mainly affects the trailing pantograph behaviour. In this section, only the trailing pantograph behaviour is analysed. The trailing pantograph PCCF statistics at different speeds with and without

damping ratio variation are presented in Figure 12. At different speeds, the damping ratio variation does not cause a distinct difference in the PCCF standard deviation. The difference in the maximum PCCF becomes significant when the train speed increases to 250 km/h. Especially at 280 km/h, the maximum PCCF evaluated without damping ratio variation is smaller than the critical safety threshold of 350 N, whereas the result with damping ratio variation exceeds the safety threshold. When the train speed exceeds 200 km/h, an evident difference in the contact loss rate can be seen. The greatest difference reaches 11.76% at 280 km/h. Note that only the mean damping coefficients at each measurement position are adopted in this analysis. The resulting PCCF should be stochastic due to the randomness of the damping coefficients. In next Section, a stochastic analysis is performed to investigate the dispersion of the standard deviation, the maximum PCCF and the contact loss rate with the damping ratio uncertainty at each point.

V. STOCHASTIC ANALYSIS OF DYNAMIC PERFORMANCE

The standard deviations in Figure 3 imply an inherent uncertainty in the identified damping ratio among the multiple measurements. When the damping ratio uncertainty is presented, the deterministic analysis in Section IV is not sufficient to fully describe the behaviour of the pantograph-catenary interactions. In this section, the damping ratio coefficients at each point are assumed to be independent Gaussian distributed variables and are therefore defined by their mean and standard deviations, which are presented in Figure 3. One widely used method to perform stochastic analysis is the MC technique [42]. The advantage of the MC method is that it takes the nonlinearities of the model into account without imposing any restrictions on the output probability distributions. However, a large number of numerical simulations are required to ensure accuracy, which entails a considerable computational cost. In [32], it was demonstrated that a very small element length should be adopted to guarantee the numerical accuracy at frequencies of up to 200 Hz, which consumes tremendous computational resources. Thus, in this analysis, a reasonable number of simulations (300) is selected to quantify the uncertainties of the results caused by the random damping ratio.

The boxplots of the PCCF standard deviation at different speeds are presented in Figure 13. The damping ratio uncertainty leads to a slight dispersion of the PCCF standard deviation. The dispersion with the 200 Hz cut-off frequency is slightly greater than that with the 20 Hz cut-off frequency for both the leading and trailing pantographs. For all cases, the dispersion increases with increasing train speed. To directly quantify the dispersion among 300 simulations, Figure 14 presents the variance of 300 simulation results of the PCCF standard deviation at different speeds. When the damping ratio uncertainty is included, the increase in the train speed causes a sharp increase in the variation in the resulting PCCF standard deviation. However, even at 280 km/h, the maximum variance only reaches 0.045 N<sup>2</sup> with a 200 Hz cut-off frequency. Therefore, the damping ratio uncertainty does not have an evident impact on the PCCF standard deviation.

The boxplots of the maximum PCCF at different speeds are presented in Figure 15. The dispersion with a 200 Hz cut-off

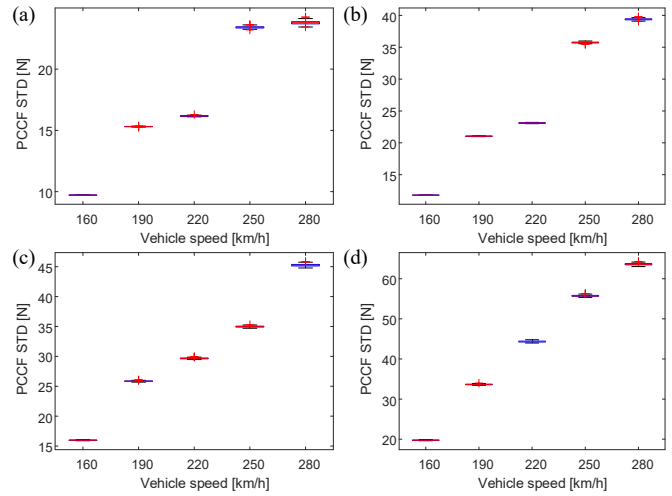


Figure 13. Boxplots of PCCF standard deviation at different speeds: (a) leading pantograph with a 20 Hz cut-off frequency, (b) trailing pantograph with a 20 Hz cut-off frequency, (c) leading pantograph with a 200 Hz cut-off frequency, and (d) trailing pantograph with a 200 Hz cut-off frequency

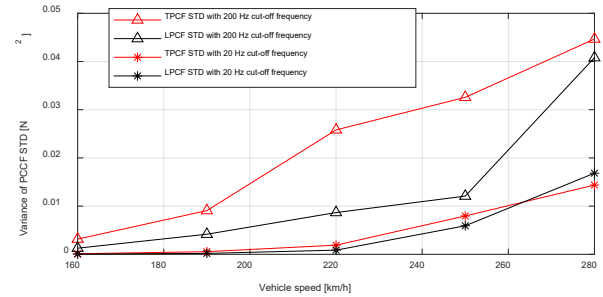


Figure 14. Variance of 300 simulation results of PCCF standard deviation at different speeds

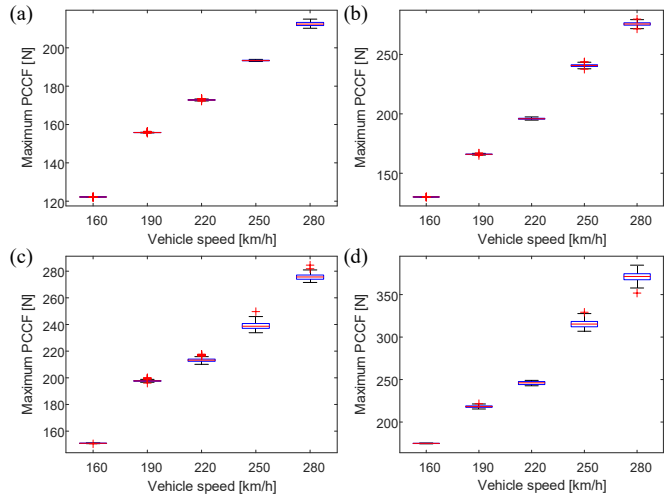


Figure 15. Boxplots of the maximum PCCF at different speeds: (a) leading pantograph with a 20 Hz cut-off frequency, (b) trailing pantograph with a 20 Hz cut-off frequency, (c) leading pantograph with a 200 Hz cut-off frequency, and (d) trailing pantograph with a 200 Hz cut-off frequency

frequency is higher than that with a 20 Hz cut-off frequency for both the leading and the trailing pantographs. Particularly, at 280 km/h, the maximum PCCF of the trailing pantograph shows a significant dispersion. According to the current standard [5], the maximum PCCF should be limited to 350 N to avoid excessive stress in the contact wire. Due to the uncertain damping of the catenary, the maximum PCCF at 280 km/h has

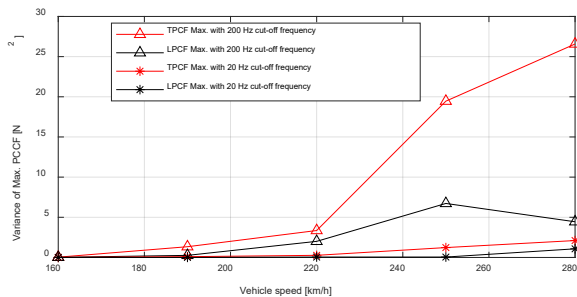


Figure 16. Variance of 300 simulation results of the maximum PCCF at different speeds

the possibility to exceed the safety threshold. Therefore, it is recommended to take the damping ratio uncertainty into account and evaluate the reliability of the pantograph-catenary interaction. Figure 16 presents the variance of 300 simulation results of the maximum PCCF at each speed. When stochastic damping is present, the increase in the train speed causes a sharp increase in the variation in the resulting maximum PCCF. At 280 km/h, the variances of the leading pantograph maximum PCCF are  $4.44 \text{ N}^2$  and  $1.08 \text{ N}^2$  with 200 Hz and 20 Hz cut-off frequencies, respectively, which result in very small variations and can be neglected in the numerical simulations. However, for the trailing pantograph, the variances of the maximum PCCF with a 200 Hz cut-off frequency reach  $19.46 \text{ N}^2$  and  $26.57 \text{ N}^2$  at 250 km/h and 280 km/h, respectively. According to the well-known three-sigma rule [43], the corresponding differences between the smallest and the largest values can reach over 24 N and 30 N ( $-3\sigma \sim 3\sigma$ ), which creates considerable deviations in evaluating the maximum PCCF. When a constant damping ratio of the catenary is used, a large error may be expected when calculating the maximum PCCF.

The boxplots of the trailing pantograph contact loss rate evaluated with a 200 Hz cut-off frequency at different speeds are presented in Figure 17. The dispersion of the contact loss rate increases with increasing speed. Generally, a higher speed causes a higher contact loss rate. However, note that a higher speed leads to a greater aerodynamic force of the pantograph, which increases the mean contact force and reduces the occurrence of contact loss. The contact loss rate at 280 km/h is therefore smaller than that at 250 km/h. Figure 18 presents the variance of 300 simulation results of trailing pantograph contact loss at each speed. When the inherent damping uncertainty is present, the increase in the train speed causes a continuous increase in the dispersion of the resulting contact loss rate. According to the three-sigma rule, the corresponding differences between the smallest and the largest values can reach over 0.12%, 0.18% and 0.21% at 220 km/h, 250 km/h and 280 km/h respectively, which create significant dispersions in evaluating the contact loss rate. In contrast, when the operating speed is lower than 220 km/h, the dispersion of the contact loss rate caused by the damping uncertainty is very small and can be neglected.

## VI. CONCLUSIONS

In previous research, the damping ratio of railway catenaries was assumed to be constant in numerical simulations. This assumption must be improved as the damping ratio along one span has been proven to vary and shows evident uncertainty at

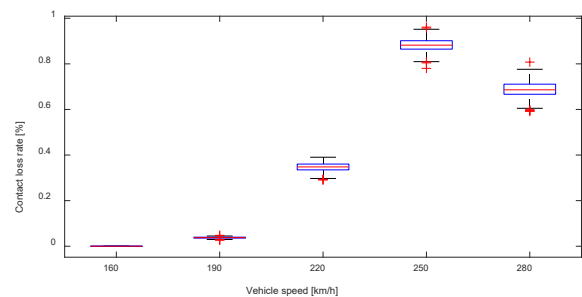


Figure 17. Boxplots of trailing pantograph contact loss with a 200 Hz cut-off frequency at different speeds

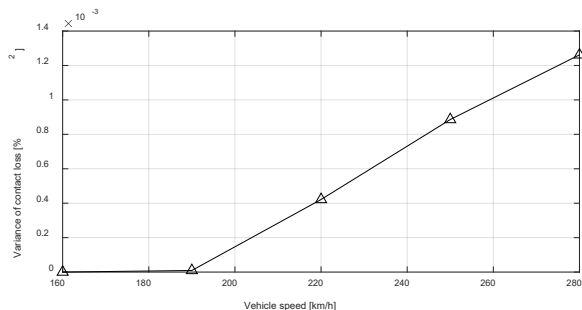


Figure 18. Variance of 300 simulation results of trailing pantograph contact loss at different speeds

each point according to field measurements. In this paper, a methodology is proposed to include the variation and uncertainty of the damping ratio in the evaluation of pantograph-catenary interaction performance. To analyse the contact loss occurring at high frequencies, a variable time step is employed to capture the accurate separation and reattachment time instants of the pantograph head and the contact wire. Through several numerical analyses, the main conclusions can be summarised as follows:

- 1) The damping ratio variation cannot affect the low-frequency performance of pantograph-catenary interactions. It is not necessary to include the damping ratio variation in the evaluation of the contact force filtered with a 20 Hz cut-off frequency according to the current standard.

- 2) When the cut-off frequency moves up to 200 Hz, some local behaviours of the contact force are significantly changed when a variable damping ratio is included. Particularly, the contact loss duration of the trailing pantograph evaluated with a constant damping ratio has significant differences from the result with a variable damping ratio.

- 3) The stochastic analysis shows that the damping ratio uncertainty should be considered when evaluating the high-frequency maximum contact force and contact loss for the trailing pantograph at high speed. For the analysis object, the damping ratio uncertainty should be considered when the train speed exceeds 220 km/h. Otherwise, a relatively large error may be expected when using a traditional constant damping ratio.

The main finding of this work is that the damping spatial distribution and uncertainty have a specific effect on the contact force with a 200 Hz cut-off frequency. The current inspection vehicle can only obtain the measured contact force with a 20 Hz cut-off frequency. The validation of the numerical simulation still requires the improvement of the measurement equipment in the future.

## REFERENCES

- [1] J. Martin, "Dynamic Modelling of Overhead Power Lines for Electric Trains," in *2018 UKACC 12th International Conference on Control, CONTROL 2018*, 2018, pp. 120–125.
- [2] D. Zou, W. H. Zhang, R. P. Li, N. Zhou, and G. M. Mei, "Determining damping characteristics of railway-overhead-wire system for finite-element analysis," *Veh. Syst. Dyn.*, vol. 54, no. 7, pp. 902–917, 2016.
- [3] Z. Xu, Y. Song, and Z. Liu, "Effective Measures to Improve Current Collection Quality for Double Pantographs and Catenary Based on Wave Propagation Analysis," *IEEE Trans. Veh. Technol.*, vol. 69, no. 6, pp. 6299–6309, 2020.
- [4] European Committee for Electrotechnical Standardization, *EN 50317: Railway applications - Current collection systems - Requirements for and validation of measurements of the dynamic interaction between pantograph and overhead contact line*. Brussels: European Standards (EN), 2012.
- [5] European Committee for Electrotechnical Standardization, *EN 50367. Railway applications — Current collection systems — Technical criteria for the interaction between pantograph and overhead line*. Brussels: European Standards (EN), 2012.
- [6] J. Ambrósio, J. Pombo, M. Pereira, P. Antunes, and A. Mósca, "Recent Developments in Pantograph-Catenary Interaction Modelling and Analysis," *Int. J. Railw. Technol.*, vol. 1, no. 1, pp. 249–278, 2012.
- [7] Y. Song, Z. Liu, F. Duan, Z. Xu, and X. Lu, "Wave propagation analysis in high-speed railway catenary system subjected to a moving pantograph," *Appl. Math. Model.*, vol. 59, pp. 20–38, 2018.
- [8] W. Zhang, G. Mei, and J. Zeng, "A study of pantograph/catenary system dynamics with influence of presag and irregularity of contact wire," *Veh. Syst. Dyn.*, vol. 37, no. SUPPL., pp. 593–604, 2003.
- [9] J. Zhang, W. Liu, and Z. Zhang, "Study on Characteristics Location of Pantograph-Catenary Contact Force Signal Based on Wavelet Transform," *IEEE Trans. Instrum. Meas.*, vol. 68, no. 2, pp. 402–411, 2019.
- [10] Y. Song, Z. Liu, H. Wang, X. Lu, and J. Zhang, "Nonlinear modelling of high-speed catenary based on analytical expressions of cable and truss elements," *Veh. Syst. Dyn.*, vol. 53, no. 10, pp. 1455–1479, 2015.
- [11] O. Vo Van, J. P. Massat, and E. Balmes, "Waves, modes and properties with a major impact on dynamic pantograph-catenary interaction," *J. Sound Vib.*, vol. 402, pp. 51–69, 2017.
- [12] Y. Yao, D. Zou, N. Zhou, G. Mei, J. Wang, and W. Zhang, "A study on the mechanism of vehicle body vibration affecting the dynamic interaction in the pantograph-catenary system," *Veh. Syst. Dyn.*, vol. 56, no. 8, pp. 1207–1232, 2020.
- [13] Y. Song, Z. Wang, Z. Liu, and R. Wang, "A spatial coupling model to study dynamic performance of pantograph-catenary with vehicle-track excitation," *Mech. Syst. Signal Process.*, vol. 151, p. 107336, 2021.
- [14] Y. Song, Z. Liu, F. Duan, X. Lu, and H. Wang, "Study on wind-induced vibration behavior of railway catenary in spatial stochastic wind field based on nonlinear finite element procedure," *J. Vib. Acoust. Trans. ASME*, vol. 140, no. 1, pp. 011010-1–14, 2018.
- [15] Y. Yao, N. Zhou, G. Mei, and W. Zhang, "Dynamic Analysis of Pantograph-Catenary System considering Ice Coating," *Shock Vib.*, vol. 2020, pp. 1–15, Sep. 2020.
- [16] M. Zhang, F. Xu, and O. Øiseth, "Aerodynamic damping models for vortex-induced vibration of a rectangular 4:1 cylinder: Comparison of modeling schemes," *J. Wind Eng. Ind. Aerodyn.*, vol. 205, 2020.
- [17] M. Zhang, F. Xu, and Y. Han, "Assessment of wind-induced nonlinear post-critical performance of bridge decks," *J. Wind Eng. Ind. Aerodyn.*, vol. 203, 2020.
- [18] Y. Song, Z. Liu, H. Wang, J. Zhang, X. Lu, and F. Duan, "Analysis of the galloping behaviour of an electrified railway overhead contact line using the non-linear finite element method," *Proc. Inst. Mech. Eng. Part F J. Rail Rapid Transit*, vol. 232, no. 10, pp. 2339–2352, 2018.
- [19] S. Derosa, P. Nāvik, A. Collina, G. Bucca, and A. Rønquist, "A heuristic wear model for the contact strip and contact wire in pantograph – Catenary interaction for railway operations under 15 kV 16.67 Hz AC systems," *Wear*, vol. 456–457, no. July, p. 203401, 2020.
- [20] Y. Song, Z. Z. Liu, A. Rønquist, P. Navik, and Z. Z. Liu, "Contact Wire Irregularity Stochastics and Effect on High-Speed Railway Pantograph-Catenary Interactions," *IEEE Trans. Instrum. Meas.*, vol. 69, no. 10, pp. 8196–8206, Oct. 2020.
- [21] Y. Song, P. Antunes, J. Pombo, and Z. Liu, "A methodology to study high-speed pantograph-catenary interaction with realistic contact wire irregularities," *Mech. Mach. Theory*, vol. 152, no. xxxx, p. 103940, May 2020.
- [22] F. Vesali, M. A. Rezvani, H. Molatefi, and M. Hecht, "Static form-finding of normal and defective catenaries based on the analytical exact solution of the tensile Euler–Bernoulli beam," *Proc. Inst. Mech. Eng. Part F J. Rail Rapid Transit*, vol. 233, no. 7, pp. 691–700, 2019.
- [23] Y. Song, Z. Liu, and X. Lu, "Dynamic Performance of High-Speed Railway Overhead Contact Line Interacting with Pantograph Considering Local Dropper Defect," *IEEE Trans. Veh. Technol.*, vol. 69, no. 6, pp. 5958–5967, 2020.
- [24] S. Gregori, M. Tur, J. E. Tarancón, and F. J. Fuenmayor, "Stochastic Monte Carlo simulations of the pantograph-catenary dynamic interaction to allow for uncertainties introduced during catenary installation," *Veh. Syst. Dyn.*, vol. 57, no. 4, pp. 471–492, 2019.
- [25] J. Zhang, W. Liu, and Z. Zhang, "Sensitivity analysis and research on optimisation methods of design parameters of high-speed railway catenary," *IET Electr. Syst. Transp.*, vol. 9, no. 3, pp. 150–156, Sep. 2019.
- [26] S. Gregori, M. Tur, E. Nadal, and F. J. Fuenmayor, "An approach to geometric optimisation of railway catenaries," *Veh. Syst. Dyn.*, vol. 56, no. 8, pp. 1162–1186, Aug. 2018.
- [27] X. Lu, Z. Liu, J. Zhang, H. Wang, Y. Song, and F. Duan, "Prior-Information-Based Finite-Frequency  $H_\infty$  Control for Active Double Pantograph in High-Speed Railway," *IEEE Trans. Veh. Technol.*, vol. 66, no. 10, pp. 8723–8733, 2017.
- [28] I. Aydin, E. Karakose, M. Karakose, M. T. Gencoglu, and E. Akin, "A new computer vision approach for active pantograph control," *2013 IEEE Int. Symp. Innov. Intell. Syst. Appl. IEEE INISTA 2013*, 2013.
- [29] P. Nāvik, A. Rønquist, and S. Stichel, "Identification of system damping in railway catenary wire systems from full-scale measurements," *Eng. Struct.*, vol. 113, pp. 71–78, 2016.
- [30] F. Duan, Z. Liu, D. Zhai, and A. Rønquist, "A siamese network-based non-contact measurement method for railway catenary uplift trained in a free vibration test," *Sensors (Switzerland)*, vol. 20, no. 14, pp. 1–17, 2020.
- [31] S. Bruni *et al.*, "The results of the pantograph-catenary interaction benchmark," *Veh. Syst. Dyn.*, vol. 53, no. 3, pp. 412–435, Mar. 2015.
- [32] Y. Song, A. Rønquist, and P. Nāvik, "Assessment of the High-Frequency Response in Railway Pantograph-Catenary Interaction Based on Numerical Simulation," *IEEE Trans. Veh. Technol.*, vol. 69, no. 10, pp. 10596–10605, 2020.
- [33] T. Jiang, G. T. Frøseth, A. Rønquist, and E. Fagerholt, "A

- robust line-tracking photogrammetry method for uplift measurements of railway catenary systems in noisy backgrounds,” *Mech. Syst. Signal Process.*, vol. 144, 2020.
- [34] P. Nāvīk, A. Rønquist, and S. Stichel, “A wireless railway catenary structural monitoring system: Full-scale case study,” *Case Stud. Struct. Eng.*, vol. 6, pp. 22–30, 2016.
- [35] C. Rainieri and G. Fabbrocino, *Operational Modal Analysis of Civil Engineering Structures*. 2014.
- [36] A. L. Schwab and J. P. Meijaard, “Comparison of three-dimensional flexible beam elements for dynamic analysis: Classical finite element formulation and absolute nodal coordinate formulation,” *J. Comput. Nonlinear Dyn.*, vol. 5, no. 1, pp. 1–10, 2010.
- [37] Y. Song, Z. Liu, Z. Xu, and J. Zhang, “Developed moving mesh method for high-speed railway pantograph-catenary interaction based on nonlinear finite element procedure,” *Int. J. Rail Transp.*, vol. 7, no. 3, pp. 173–190, 2019.
- [38] W. J. Qian, G. X. Chen, W. H. Zhang, H. Ouyang, and Z. R. Zhou, “Friction-induced, self-excited vibration of a pantograph-catenary system,” *J. Vib. Acoust. Trans. ASME*, vol. 135, no. 5, p. 051021, 2013.
- [39] European Committee for Electrotechnical Standardization, *EN 50318. Railway applications - Current collection systems - Validation of simulation of the dynamic interaction between pantograph and overhead contact line*. Brussels: European Standards (EN), 2018.
- [40] P. Nāvīk, A. Rønquist, and S. Stichel, “Variation in predicting pantograph–catenary interaction contact forces, numerical simulations and field measurements,” *Veh. Syst. Dyn.*, vol. 55, no. 9, pp. 1265–1282, 2017.
- [41] European Committee for Electrotechnical Standardization, *EN 50119. Railway applications — Fixed installations — Electric traction overhead contact lines*. Brussels: European Standards (EN), 2013.
- [42] A. Barbu and S. C. Zhu, *Monte carlo methods*, 1st ed. Singapore: Springer Singapore, 2020.
- [43] Pukelsheim, “The three sigma rule,” *Am. Stat.*, vol. 48, no. 2, pp. 88–91, 1994.